Mass-anisotropy splitting of indirect excitons in diamond

Yuji Hazama and Nobuko Naka*
Department of Physics, Kyoto University, Kitashirakawa-Oiwake-cho, Sakyo-ku, Kyoto 606-8502, Japan

Heinrich Stolz
Institut für Physik, Universität Rostock, D-18051 Rostock, Germany
(Received 9 May 2014; published 30 July 2014)

We have investigated fine structure splitting of indirect excitons in ultrapure diamond by high-resolution spectroscopy. The role of the mass-anisotropy splitting has been revealed by comparison with group-theoretical calculations of the reduced matrix elements for phonon scattering of electrons and holes followed by the radiative recombination. The observed energy levels and coupling strengths of the fine structure states are successfully reproduced by inclusion of the mass-anisotropy splitting in addition to the exchange and spin-orbit interactions.

DOI: 10.1103/PhysRevB.90.045209 PACS number(s): 71.35.Cc, 71.70.−d

I. INTRODUCTION

Diamond is known for the extremely long spin coherence time of localized electrons at nitrogen-vacancy centers [1]. The long coherence time originates from the unique band structure of diamond, in which the spin-orbit splitting is much smaller than the energy scale of the electronic excitations so that the electrons are kept free from the spin flip. The small spin-orbit splitting brings a complex situation that the split-off hole bands cannot be ignored in the valence band structure as usually done for conventional semiconductors. Therefore, effects of the exchange interaction on electronic excitations such as excitons in the presence of the small spin-orbit interaction in diamond is a subject of controversy.

Experimentally, there were several challenges to directly observe fine structure states of excitons in diamond. In cyclotron resonance measurements the splitting of the hole bands was measured as ∼6 meV [2]. Dean *et al.* [3] first found a doublet structure of excitons in the cathodoluminescence spectra. The two components separated by 7 meV were interpreted to be due to the spin-orbit splitting of the valence bands. Sauer *et al.* later found two groups of levels by jointly analyzing photoluminescence and absorption spectra [4,5]. The separation of 10.3 meV between the two groups with each made up of four lines was interpreted as an exchange interaction which dominates over the spin-orbit interaction. On the other hand, Cardona *et al.* [6] extracted a different outcome based on the spectral weights [7] of the same spectra: the spin-orbit interaction of 11.7 meV [8,9], which is larger than the exchange interaction estimated as 3.9 meV.

Recently, another possibility which can further complicate the situation is found by the direct determination of the effective masses of electron and hole bands in intrinsic diamond [10]. The extracted values of the anisotropic electron effective masses and Luttinger parameters for the hole bands imply that the excitonic fine structure can be affected by another kind of interaction. That is mass-anisotropy splitting originating from the mass anisotropy of electrons into directions along or perpendicular to the conduction valley axis as well as from the anisotropy of the hole effective masses. The mass-anisotropy splitting was so far observed in germanium (1 meV) and expected for silicon (0.5 meV) [11], but had never been discussed for diamond and under competition with exchange interaction. A simple estimation [11] for diamond gives mass-anisotropy splitting of 3.2 meV, which can compete with exchange and spin-orbit interactions of the same order.

Such fine energy splittings should be clarified by precise spectral information in the deep ultraviolet region for diamond having the large band gap. Due to the indirect nature of the band gap, a direct optical transition at the Γ point is forbidden and transitions involving participation of phonons are allowed. Generally, a phonon-assisted recombination line has a wider spectral width than a zero-phonon recombination line. In addition, heating of the electronic system during excitation of diamond [3,12] causes thermal broadening of the photoluminescence spectrum and overlap of the fine structure peaks. Therefore, interpretation of the spectra of indirect excitons in diamond was not straightforward. Recently, we have developed an excitation method which selectively creates cold excitons [13,14]. It is now possible to observe the fine structure splitting directly at the photoluminescence spectra with minimal thermal broadening.

In this paper, we present the excitonic fine structure observed with four-level splitting. We calculate the transition matrix elements for the phonon-assisted recombination of each fine structure state involving transverse acoustic (TA), transverse optical (TO), longitudinal optical (LO), and longitudinal acoustic (LA) phonons by using the second-order perturbation theory. The quantitative comparison of the observations with the theory indicates that the mass-anisotropy splitting plays a crucial role in competition with the exchange and spin-orbit interactions.

II. EXPERIMENTAL RESULTS

Figure 1 shows a spectrum of phonon-assisted recombination of excitons in a chemical-vapor-deposition single crystal of diamond at 1.8 K. The high spectral resolution was achieved by the use of a monochromator of 1500 mm focal length and of a CCD camera with small pixel size, 13.5 μm. The excitons with minimum kinetic energy were photogenerated near the phonon-assisted absorption edge [14]. Excitonic emission lines due to four different phonon modes, i.e., LO, TO, LA,

*naka@scphys.kyoto-u.ac.jp

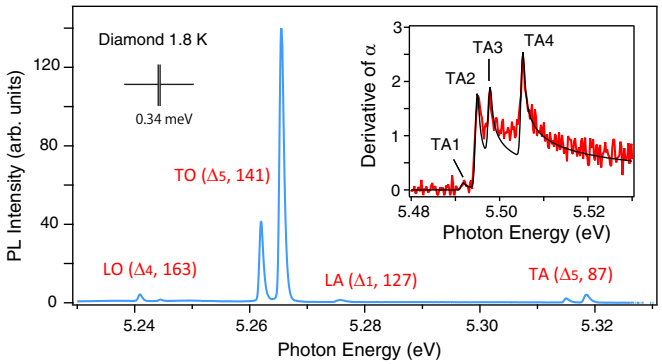

FIG. 1. (Color online) Photoluminescence spectrum of excitons in high-purity diamond at 1.8 K. Labels within the parentheses show phonon modes with respective symmetry and energy in units of meV. Inset: derivative of an absorption spectrum around the TA phonon-assisted edge.

and TA phonons are seen. The TO-phonon assisted line has the largest amplitude, while other phonon lines are weaker by a factor of ∼20. The splitting of the excitonic levels into two components is clearly seen for the LO, TO, and TA lines.

The inset in Fig. 1 shows a derivative of an absorption spectrum of the TA-phonon assisted transition. The derivative indicates four levels due to fine structure splitting. We refer to the corresponding phonon absorption edges as TA1, TA2, TA3, and TA4, from low to high energies. The black line represents the spectral analysis similar to that performed for silicon [15]. The result gives the relative amplitudes of the phonon-assisted transitions for each fine structure state, that are obtained as 0.074, 1.0, 0.74, and 1.1. The TA1 line has a very small amplitude, implying that the lowest fine structure state is not a bright state.

Similar analysis for TO-phonon assisted absorption was impossible because of the strong absorption at higher energies. Therefore, we analyze the photoluminescence spectra to extract the transition rates. It is assumed that the excitonic lifetime is comparable to the duration (2.5 ns) of the excitation laser pulses and is long enough to establish quasithermal equilibrium between the fine structure levels [14]. Figure 2(a) shows the spectra of TO-phonon assisted recombination at various lattice temperatures. At low temperatures, splitting of the excitonic levels into two components (TO1, TO2) is clearly seen. With the increase of the lattice temperature, the spectrum is broadened by the thermal population of excitons into higher kinetic energy states. Furthermore, two additional components appear at higher energies (as labeled in the figure by TO3 and TO4). Therefore, we fit each spectrum with a four-component Maxwell Boltzmann distribution, $\sum_{i=1,2,3,4} A_i(T)\sqrt{E-E_i}\exp[-(E-E_i)/k_BT]$. The energy positions $E_i (i = 2,3,4)$ and the amplitudes $A_i(T) = a_i \exp[-(E_i - E_1)/k_BT]$ were varied as adjustable parameters, while the separation $E_2 - E_1$ was fixed to the value for the lowest temperature. We obtained perfect fits to the data for all the temperatures as shown by the dotted lines.

The energy positions, E_1, E_2, E_3, E_4, obtained from fits are plotted in Fig. 2(b) as a function of temperature. The black lines represent temperature shifts of the exciton energy, extrapolated below 100 K by three different methods [16]

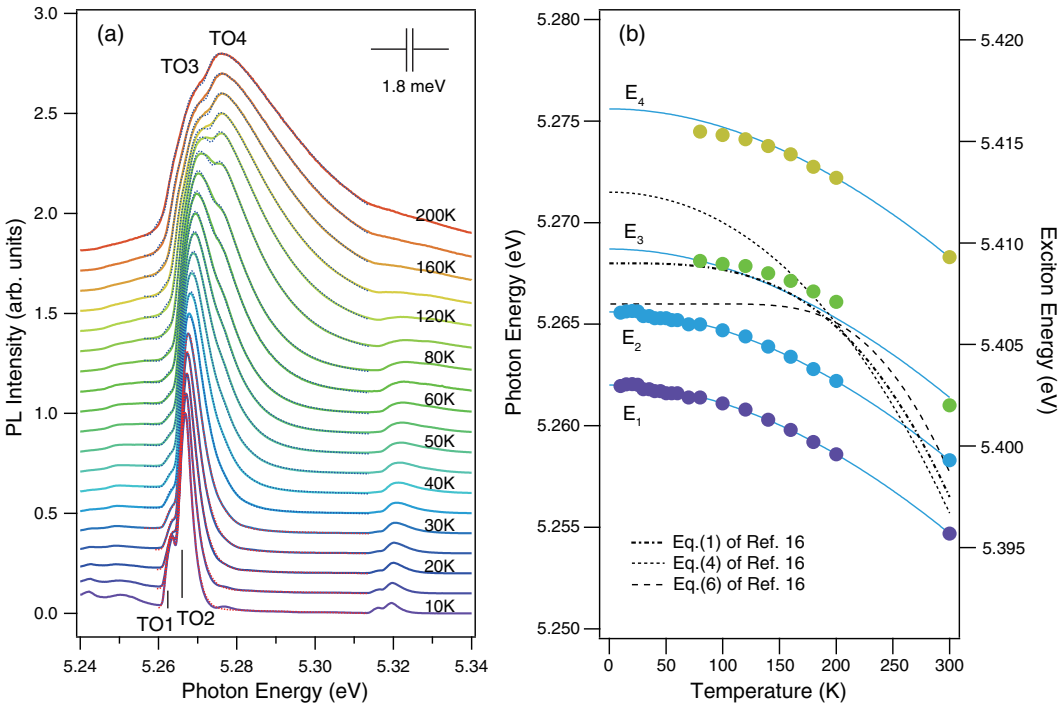

FIG. 2. (Color online) (a) Photoluminescence spectra of TO-phonon assisted recombination of excitons at various lattice temperatures. The full lines are measured spectra and the dotted lines are fits assuming four excitonic levels with different transition probabilities. (b) Temperature dependence of the energy positions of the four exciton components. The energy of TO phonon, 0.141 eV, is added so that the right vertical axis shows the exciton energy.

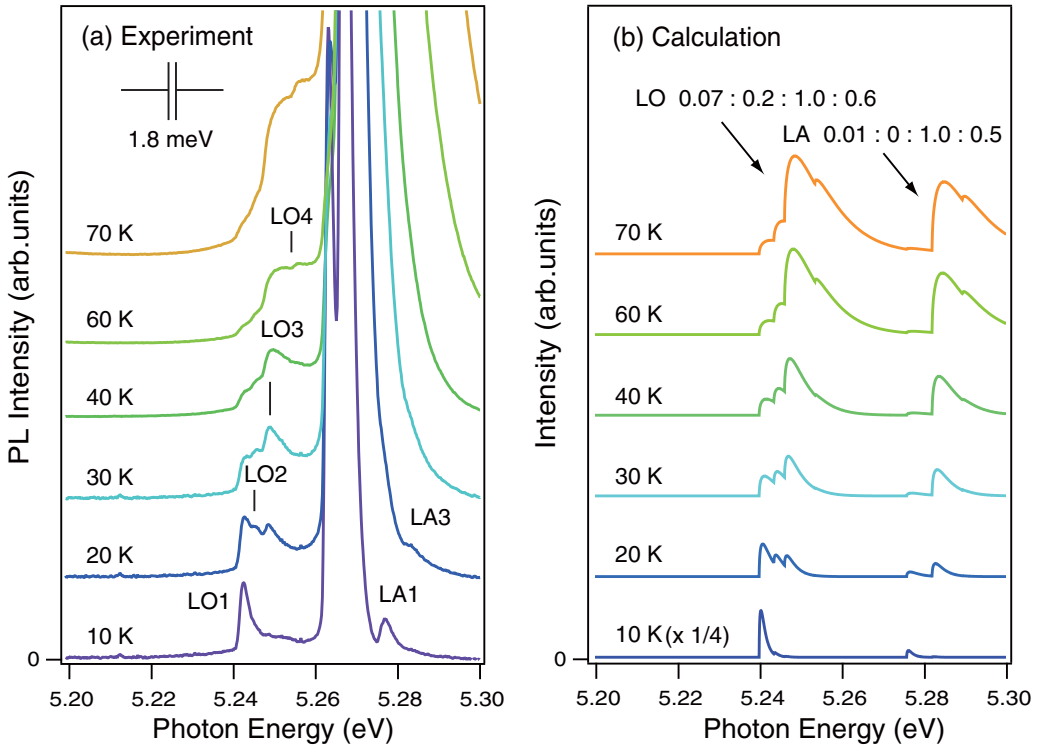

FIG. 3. (Color online) Photoluminescence spectra of LO and LA phonon assisted recombination. (a) Experimental and (b) simulated spectra for different lattice temperatures. In (b), the temperature shift of the energy positions is neglected for simplicity.

based on the reported values above 100 K. The middle one (the dashed dotted line) is close to E_3 below 200 K. The thin solid lines are guides to the present data with Varshni's empirical formula, $E_i(T) = E_i(0) - \alpha T^2/(T+\beta)$, where $E_1(0) = 5.262$ eV, $\alpha = 0.18$ meV/K, and $\beta = 1860$ K. Although invalidness for high temperatures is pointed out in Ref. [16], the empirical formula gives better fits to the data in the present temperature range. It is found that the energy separations of the four components are independent of temperature. We extracted $E_2 = 3.6$ meV, $E_3 = 6.7$ meV, and $E_4 = 13.6$ meV, as measured from the position E_1 of the lowest-energy component. The previous observation of 10.3 meV splitting at 80 K by Sauer *et al.* [4] corresponds to the separation between E_2 and E_4, and the 7 ± 2 meV splitting observed at 100 K by Dean *et al.* [3] corresponds to the separation between E_3 and E_4. The relative amplitudes, a_i, are found to be 0.03, 1.0, 0.6, and 0.9, for $i = 1,2,3,4$, respectively.

Figure 3(a) shows expanded spectra for LO and LA phonon assisted lines at various lattice temperatures. Figure 3(b) shows simulated curves with fixed parameters E_i and a_i ($i = 1,2,3,4$). The intensity ratios for the LO1–LO4 lines are found to be 0.07, 0.2, 1.0, and 0.6. Those for the LA1–LA4 lines are 0.01, 0, 1.0, and 0.5, where the LA phonon energy of 127 meV is assumed.[1] These ratios are clearly different from those for TO and TA lines.

[1]This value is consistent with the neutron scattering measurement [22] and our absorption data, although by 5 meV different from the value reported in Ref. [23].

III. THEORY

In this section we discuss the origin of the fine structure splitting. Throughout this paper, we use the notations by Koster [17]. The hole bands with the symmetry of Γ_5^+ in diamond consist of twofold $j = 1/2$ (Γ_7^+) bands and fourfold $j = 3/2$ (Γ_8^+) bands, where j is the total angular momentum for holes. The separation between these bands gives the spin-orbit splitting, E_{so}. The holes couple to electrons in the Δ_1 valleys by Coulomb interaction to form *indirect* excitons. Considering the spin of electrons (up or down) and six hole states explained above, there should be 12 excitonic states.

When considering the emission intensity of each state, we should note that the argument of the spectral weights of direct transitions in alkali halides [7] is not directly applicable to diamond, because the recombination of indirect excitons involves phonons. We calculate the transition matrix elements for phonon-assisted recombination of indirect excitons by the second-order perturbation theory for holes in the $j = 3/2, 1/2$ bands and electrons in a Δ_1 valley. To perform the calculation, we extended the method known for silicon [15,18] to cover the $j = 1/2$ (split-off) hole bands.

There exist several phonon-assisted transition channels in diamond. Possible scattering channels for small energy denominators are summarized in Table I. The conduction band (c.b.) scattering of an electron from the Δ_1 valley to the Γ point of the Γ_4^- band, followed by a dipole transition between the Γ_4^- conduction and the Γ_5^+ valence bands, is allowed. The valence band (v.b.) scattering of a hole from the top of the Γ_5^+ to the Δ_5 bands, followed by a dipole transition to the Δ_1 conduction valley, can also occur. In addition, interband scattering from Δ_1 to Γ_2^- conduction bands and

TABLE I. Possible channels for phonon scattering. The subscripts to the reduced matrix elements indicate the modes of the phonons for allowed scattering.

Channels	Energy (eV)	Matrix element
intra c.b. ($\Delta_1 \to \Gamma_4^-$)	1.00	$W_{\mathrm{TO,TA,LA}}$
intra v.b. ($\Gamma_5^+ \to \Delta_5$)	6.66	$Q_{\mathrm{TO,TA,LO,LA}}$
inter c.b. ($\Delta_1 \to \Gamma_2^-$)	11.52	S_{LO}
inter v.b. ($\Gamma_5^+ \to \Delta_1$)	13.16	$U_{\mathrm{TO,TA,LO}}$

that from Γ_5^+ to Δ_1 valence bands also occur, although the energy denominators are somewhat larger. A matrix element for a phonon-assisted transition is given by the sum of these contributions: $M = W + Q + S + U$, where

$$W(S) = \frac{\langle \Gamma_5^+ | e \cdot p | \Gamma_{4(2)}^- \rangle \langle \Gamma_{4(2)}^- | H_p | \Delta_1 \rangle}{E^c_{\Delta_1} - E^c_{\Gamma_{4(2)}^-} \pm \hbar\omega_p},$$

$$Q(U) = \frac{\langle \Gamma_5^+ | H_p | \Delta_{5(1)} \rangle \langle \Delta_{5(1)} | e \cdot p | \Delta_1 \rangle}{E^v_{\Gamma_5^+} - E^v_{\Delta_{5(1)}} \pm \hbar\omega_p}.$$

Here, $e \cdot p$ denotes the exciton-photon interaction of dipole type, H_p exciton-phonon interaction, and $\hbar\omega_p$ phonon energy. The energy denominators can be taken according to theoretical values in Ref. [19] as summarized in Table I, where the phonon energies are neglected. The transition matrix elements for 12 exciton states are summarized in Table III in the Appendix for different polarizations X, Y, and Z of the emitted photons.

IV. LEVEL ASSIGNMENTS

Figures 4(a) and 4(b) illustrate splitting of the exciton levels by the spin-orbit interaction of the valence bands. To account for the observed splitting, we further include the splitting of the Γ_8^+ valence bands by mass-anisotropy splitting [11,20] [Fig. 4(c)]. This splitting originates from the fact that electrons in conduction bands take the energy minimum at the Δ points, where the effective mass is different in a direction along or perpendicular to the [001] crystal axis ($m_l = 1.56$ and $m_t = 0.280$ in units of the free electron mass) [10]. The symmetry of the exciton wave function is determined by the direct product of the representations for the envelope, hole, and electron functions. Here, we drop the envelope representation because we are concerned with $1s$ excitons only. The resulting symmetry for $j = 3/2$ components is $\Gamma_8^+ \otimes \Delta_1 = \Delta_6 \oplus \Delta_7$, giving rise to the splitting into two levels. According to the axial model by Lipari and Altarelli [11], the separation is given by $2\delta_m = (64/5)\mu_{01}\gamma_2\mu_0 S_1(0) Ry = 3.2$ meV, where $\mu_0 = 3/(2/m_t + 1/m_l + 3\gamma_1)$, $\mu_{01} = (1/m_t - 1/m_l)\mu_0/3$, $S_1(0) = 0.2246$, and exciton Rydberg energy $Ry = 80$ meV with Luttinger parameters $\gamma_1 = 2.67$ and $\gamma_2 = -0.40$ [10] for the hole bands. Because γ_2 is positive in silicon and negative in diamond [10], the order of Δ_6 and Δ_7 levels should be opposite in the two materials. In diamond the heavy-hole excitons are located at a higher energy than the light-hole excitons. This kind of splitting does not arise for the $j = 1/2$ (split-off) valence bands having the Γ_7^+ symmetry, because the corresponding exciton state has a single symmetry of $\Gamma_7^+ \otimes \Delta_1 = \Delta_7$. However, these three levels as shown in

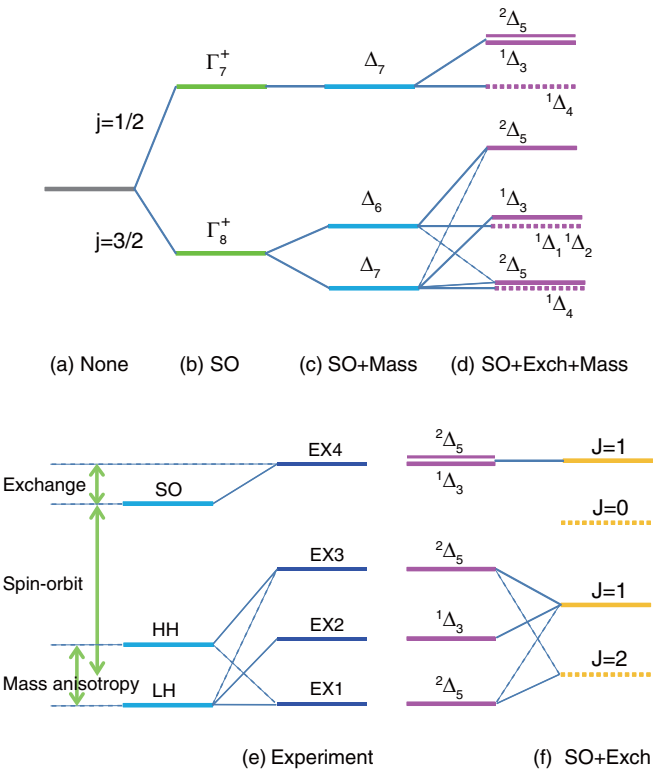

FIG. 4. (Color online) Schematic diagram explaining the splitting of excitonic states. Dark states are represented by dashed lines. (a) Valence bands without spin-orbit splitting; (b) valence band splitting by spin-orbit interaction; (c) excitonic levels with spin-orbit interaction with mass-anisotropy splitting; (d) excitonic levels with spin-orbit and exchange interactions with mass-anisotropy splitting; (e) correspondence between experimentally observed levels and optically allowed states; (f) excitonic levels with spin-orbit and exchange interaction. $J = j + s$, where $s = \pm 1/2$ is the electron spin.

Fig. 4(c) do not explain the observed four-level fine structure. By turning on a small exchange interaction, $E_{\mathrm{ex}} (< E_{\mathrm{so}})$, each group splits into sublevels leading to eight levels in total. Inclusion of the electron wave functions with spins of Δ_6 symmetry gives rise to the representations of the resulting exciton states as shown in Fig. 4(d), where dotted lines indicate optically dark states.

By comparing the experimental result [Fig. 4(e)] with the theoretical expectation, we assigned EX1–EX4 to $^2\Delta_5$, $^1\Delta_3$,$^2\Delta_5$, and $\{^1\Delta_3,^2\Delta_5\}$, respectively. Then, EX1 and EX2 come from light hole, while EX3 and EX4 come from heavy hole and split-off hole, respectively. For EX1 and EX3, the light- and heavy-hole bands slightly mix each other. When calculating the transition rates, we summed the transition matrix elements over states having the same energy, took the square of the amplitudes, and then summed over X, Y, and Z polarizations. The calculations were first performed under simplified conditions assuming no mixing between split-off and other hole bands, no difference in the masses of the hole bands, and without mass anisotropy splitting ($E_{\mathrm{so}} \gg E_{\mathrm{ex}} \gg \delta_m$; see Appendix). The reduced matrix elements for phonon-assisted recombination for each phonon mode are given in Table II in comparison with the experimental values.

TABLE II. Parameters on the fine structure obtained by the line shape analysis. Values in angle brackets mean that they are extracted based on absorption spectra, while others based on photoluminescence spectra. "Calc." means calculated transition probabilities in the limit of $E_{so} \gg E_{ex} \gg \delta_m$. $A_x = 2/3(Q_{Tx} + W_{Tx})^2, B_x = 2/3(W_{Tx} + \sqrt{2}U_{Tx})^2$ with $x = A$ or O, $C = 4/9(S_{LO} + \sqrt{3}U_{LO})^2, D = 2/9(2S_{LO} + \sqrt{3}Q_{LO})^2, E = 2/3(Q_{LA} + \sqrt{2}W_{LA})^2$, where W, Q, S, U are defined as in the text.

	EX1	EX2	EX3	EX4
E_i(TA)	[0]	[3.4]	[6.1]	[13.5]
E_i(TO)	0	3.6	6.7	13.6
a_i(TA)	[0.074]	[1.0]	[0.74]	[1.1]
a_i(TO)	0.03	1.0	0.6	0.9
Calc.	0	A	B	$(A+B)/2$
a_i(LO)	0.07	0.2	1.0	0.6
Calc.	0	C	D	$(C+D)/2$
a_i(LA)	0.01	0	1.0	[0.5]
Calc.	0	0	E	$E/2$
Symmetry	$^2\Delta_5$	$^1\Delta_3$	$^2\Delta_5$	$^1\Delta_3, ^2\Delta_5$
Hole band	LH (HH)	LH	HH (LH)	SO

The amplitudes of the TO(TA) phonon-assisted lines for EX2, EX3, and EX4 are consistent with the calculated transition probabilities, if we assume $A \simeq 1.7B (A \simeq 1.4B)$. Similarly, the amplitudes of the LO phonon-assisted lines are well reproduced by the calculated transition probabilities, if we assume $C = 0.2D$. The very weak luminescence from EX1 is an effect of a finite δ_m on the mixing between the heavy and light hole bands. The two oscillators cancel each other for the case of $\delta_m = 0$ with C_{4v} symmetry. On the other hand, the mixing amplitudes of the light and heavy hole bands change under a finite δ_m. We estimated that the lowest Δ_5 (EX1) states acquire 10.9% of the oscillator strength of the middle Δ_5 (EX3) states, when δ_m is taken as the same amplitude as E_{ex}.

As shown in Fig. 4(f), by turning off the mass-anisotropy splitting under spin-orbit and exchange interactions of comparable magnitudes, the states can be labeled by the total angular momentum, $J = j + s$, where $s = \pm 1/2$ is the electron spin. This picture gives a clue to specify the spin nature of each fine structure state. If a positive exchange energy is assumed, the $J = 2,1,0,1$ states appear in the order of low to high energy [7]. Our calculation shows that spin-triplet ($J = 0,2$) states are optically forbidden even with inclusion of phonons in the transitions, and that only two $J = 1$ states are luminous because they contain spin-singlet component. Inclusion of the mass-anisotropy splitting splits the lower $J = 1$ states into $^1\Delta_3$ (EX2) and $^2\Delta_5$ (EX3). These states are bright states of singlet-triplet mixture. In addition, EX3 state exhibits mixing with the $^2\Delta_5$ (EX1) of the $J = 2$ states. Due to this mixing, EX1 acquires small spin-singlet component and becomes weakly luminous.

The above interpretation fully explains the observed energy splitting and the intensity ratios of the fine structure components. However, within the present experiment, we cannot identify the energy positions of the dark states that are represented by dashed lines in Fig. 4(d). In order to confirm the level assignments for these states, further experiments using external fields are in progress. In general, a spin-triplet state has a long recombination time, so influence of the spin configuration on the stability of the few-body bound states of excitons and condensation into the electron-hole liquid [21] would be an interesting direction of future study.

V. CONCLUSION

We have proposed an interpretation of the four-level splitting of the indirect excitons at the Δ point in diamond, which was revealed by high-resolution spectroscopy on absorption and photoluminescence. The model assuming the spin-orbit, exchange, and mass-anisotropy splitting predicts the eight fine structure levels consisting of 12 exciton states. The phonon-assisted transition rates involving TO, TA, LO, and LA phonons are well reproduced by the calculations using the second-order perturbation theory, indicating the significance of the mass-anisotropy splitting in the presence of exchange and spin-orbit interactions. Our present study provided a clear-cut proof to solve the long-standing controversy on the excitonic fine structure in diamond, and shed light on future utilization of the fine structure with identified spin states.

ACKNOWLEDGMENTS

This work was supported in part by JSPS KAKENHI (Grant No. 26400317) and by the Deutsche Forschungsgemeinschaft (SFB 652). N.N. thanks Tetsuto Kitamura and Makoto Kuwata-Gonokami (The University of Tokyo) for early collaboration on the photoluminescence study which triggered this work, and Kikuo Cho for fruitful discussion on short-range and long-range exchange interactions during the project supported by PRESTO (JST).

APPENDIX: CALCULATION OF THE TRANSITION PROBABILITIES

We calculated the reduced matrix elements for 12 excitonic states (without mass-anisotropy, exchange, and spin-orbit interactions) as listed in Table III. Definitions of the basis functions for holes were taken from Ref. [17] for Γ_5 (hole band) $\otimes$ Γ_6 (spin):

$$\phi^8_{-1/2} = +\frac{i}{\sqrt{2}}yz\uparrow - \frac{1}{\sqrt{2}}xz\uparrow,$$
$$\phi^8_{-3/2} = -\frac{i}{\sqrt{6}}yz\downarrow + \frac{1}{\sqrt{6}}xz\downarrow + \frac{i\sqrt{2}}{\sqrt{3}}xy\uparrow,$$
$$\phi^8_{+3/2} = +\frac{i}{\sqrt{6}}yz\uparrow + \frac{1}{\sqrt{6}}xz\uparrow + \frac{i\sqrt{2}}{\sqrt{3}}xy\downarrow,$$
$$\phi^8_{+1/2} = -\frac{i}{\sqrt{2}}yz\downarrow - \frac{1}{\sqrt{2}}xz\downarrow,$$
$$\psi^7_{+1/2} = -\frac{i}{\sqrt{3}}yz\downarrow + \frac{1}{\sqrt{3}}xz\downarrow - \frac{i}{\sqrt{3}}xy\uparrow,$$
$$\psi^7_{-1/2} = -\frac{i}{\sqrt{3}}yz\uparrow - \frac{1}{\sqrt{3}}xz\uparrow + \frac{i}{\sqrt{3}}xy\downarrow.$$

Here, upward (downward) arrow means spin up (down), and xy, yz, zx are spatial parts of the wave functions. Note that Koster's $\phi^8_{\pm 1/2}$ and $\phi^8_{\pm 3/2}$ correspond to heavy hole with symmetry Δ_6 and light hole with symmetry Δ_7, respectively.

TABLE III. Reduced matrix elements for conduction and valence band scattering. X, Y, and Z in the first row indicate the polarization of emitted photons. X and Y in superscripts mean X- and Y-polarized phonons for Tx ($x = A, O$) phonon scattering. Matrix elements for another six bases with positive m_j can be obtained by using the time-reversal operation.

j	$\phi(\psi)_{m_j}s$	X	Y	Z
3/2	$\phi^8_{-1/2}\downarrow$	0	0	0
3/2	$\phi^8_{-1/2}\uparrow$	$-1/2(W_{\rm LA}) - i/\sqrt{6}(S_{\rm LO})$	$-i/2(W_{\rm LA}) - 1/\sqrt{6}(S_{\rm LO})$	$1/2\sqrt{2}\big(-W^X_{Tx} - iW^Y_{Tx}\big)$
3/2	$\phi^8_{-3/2}\downarrow$	$1/2\sqrt{3}(W_{\rm LA}) + i/3\sqrt{2}(S_{\rm LO})$	$+i/2\sqrt{3}(W_{\rm LA}) + 1/3\sqrt{2}(S_{\rm LO})$	$1/2\sqrt{6}\big(W^X_{Tx} + iW^Y_{Tx}\big)$
3/2	$\phi^8_{-3/2}\uparrow$	$-i/\sqrt{6}\big(W^Y_{Tx}\big)$	$-i/\sqrt{6}\big(W^X_{Tx}\big)$	$-i\sqrt{2}/3(S_{\rm LO})$
1/2	$\psi^7_{-1/2}\downarrow$	$-i/2\sqrt{3}\big(W^Y_{Tx}\big)$	$-i/2\sqrt{3}\big(W^X_{Tx}\big)$	$-i/3(S_{\rm LO})$
1/2	$\psi^7_{-1/2}\uparrow$	$-1/\sqrt{6}(W_{\rm LA}) + i/3(S_{\rm LO})$	$+i/\sqrt{6}(W_{\rm LA}) - 1/3(S_{\rm LO})$	$1/2\sqrt{3}\big(-W^X_{Tx} + iW^Y_{Tx}\big)$
3/2	$\phi^8_{-1/2}\downarrow$	0	0	0
3/2	$\phi^8_{-1/2}\uparrow$	$1/2\sqrt{2}(-iQ_{\rm LA} - Q_{\rm LO})$	$1/2\sqrt{2}(-Q_{\rm LA} - iQ_{\rm LO})$	$1/2\big(-U^X_{Tx} - iU^Y_{Tx}\big)$
3/2	$\phi^8_{-3/2}\downarrow$	$1/2\sqrt{6}(+iQ_{\rm LA} + Q_{\rm LO})$	$1/2\sqrt{6}(+Q_{\rm LA} + iQ_{\rm LO})$	$1/2\sqrt{3}\big(U^X_{Tx} + iU^Y_{Tx}\big)$
3/2	$\phi^8_{-3/2}\uparrow$	$-i/\sqrt{6}\big(Q^Y_{Tx}\big)$	$-i/\sqrt{6}\big(Q^X_{Tx}\big)$	$-i\sqrt{2/3}(U_{\rm LO})$
1/2	$\psi^7_{-1/2}\downarrow$	$-i/2\sqrt{3}\big(Q^Y_{Tx}\big)$	$-i/2\sqrt{3}\big(Q^X_{Tx}\big)$	$-i/\sqrt{3}(U_{\rm LO})$
1/2	$\psi^7_{-1/2}\uparrow$	$1/2\sqrt{3}(+iQ_{\rm LA} - Q_{\rm LO})$	$1/2\sqrt{3}(-Q_{\rm LA} + iQ_{\rm LO})$	$1/\sqrt{6}\big(-U^X_{Tx} + iU^Y_{Tx}\big)$

$\psi^7_{\pm1/2}$ represent wave functions for split-off hole bands. In referring to the excitonic states by the notation $\phi(\psi)_{m_j}s$ with $s = \uparrow$ or $\downarrow$, we performed time-reversal operation on the electron spin of the Koster's bases for a two-electron system rather than on the hole states.

Then, we calculated the eigenvalues and eigenvectors diagonalized for the following Hamiltonian including mass-anisotropy, spin-orbit, and exchange interactions, where unperturbed bases were taken in the order of $\phi^8_{-1/2}\downarrow$, $\phi^8_{-1/2}\uparrow$, $\phi^8_{-3/2}\downarrow$, $\phi^8_{-3/2}\uparrow$, $\phi^8_{+3/2}\downarrow$, $\phi^8_{+3/2}\uparrow$, $\phi^8_{+1/2}\downarrow$, $\phi^8_{+1/2}\uparrow$, $\psi^7_{+1/2}\downarrow$, $\psi^7_{+1/2}\uparrow$, $\psi^7_{-1/2}\downarrow$, and $\psi^7_{-1/2}\uparrow$. Symbols for exchange integrals mean $a = 2F^*_{hh}(0)F_{hh}(0)v_{sz}$, $b = 2F^*_{lh}(0)F_{lh}(0)v_{sz}$, $c = 2F^*_{hh}(0)F_{lh}(0)v_{sz}$, $d = 2F^*_{\rm so}(0)F_{\rm so}(0)v_{sz}$, $e = 2F^*_{\rm so}(0)F_{hh}(0)v_{sz}$, and $f = 2F^*_{\rm so}(0)F_{lh}(0)v_{sz}$, where $F(0)$ is the envelope function at $r = 0$ and $v_{sz} = \int dr\, dr' a^*_s(r)a_z(r)v(r-r')a^*_z(r')a_s(r')$ is the intra-atomic exchange energy with the screened Coulomb potential v [24]:

$$H_{\rm tot} = \begin{pmatrix}
\delta_m & & & & & & & & & & & \\
 & \delta_m+\frac{a}{2} & -\frac{c}{2\sqrt{3}} & & & & & -\frac{e}{\sqrt{6}} & & & & \\
 & -\frac{c}{2\sqrt{3}} & -\delta_m+\frac{b}{6} & & & & & +\frac{f}{3\sqrt{2}} & & & & \\
 & & & -\delta_m+\frac{b}{3} & +\frac{b}{3} & & & & -\frac{f}{3\sqrt{2}} & +\frac{f}{3\sqrt{2}} & & \\
 & & & +\frac{b}{3} & -\delta_m+\frac{b}{3} & & & & -\frac{f}{3\sqrt{2}} & +\frac{f}{3\sqrt{2}} & & \\
 & & & & & -\delta_m+\frac{b}{6} & -\frac{c}{2\sqrt{3}} & & & & -\frac{f}{3\sqrt{2}} & \\
 & & & & & -\frac{c}{2\sqrt{3}} & \delta_m+\frac{a}{2} & & & & +\frac{e}{\sqrt{6}} & \\
 & & & & & & & \delta_m & & & & \\
 & -\frac{e}{\sqrt{6}} & +\frac{f}{3\sqrt{2}} & & & & & E_{\rm so}+\frac{d}{3} & & & & \\
 & & & -\frac{f}{3\sqrt{2}} & -\frac{f}{3\sqrt{2}} & & & & E_{\rm so}+\frac{d}{6} & -\frac{d}{6} & & \\
 & & & +\frac{f}{3\sqrt{2}} & +\frac{f}{3\sqrt{2}} & & & & -\frac{d}{6} & E_{\rm so}+\frac{d}{6} & & \\
 & & & & & -\frac{f}{3\sqrt{2}} & +\frac{e}{\sqrt{6}} & & & & E_{\rm so}+\frac{d}{3} &
\end{pmatrix}.$$

The calculations were first performed under a simplified condition assuming no difference in the masses of the hole bands ($a = b = c = d = E_{\rm ex}$), no mixing between split-off and other hole bands ($e = f = 0$), and without mass anisotropy splitting ($\delta_m = 0$). Wave functions for the excitonic states which diagonalize $H_{\rm tot}$ with this simplified condition are as follows:

$$\Delta_5 = \psi^7_{-1/2}\uparrow, \psi^7_{+1/2}\downarrow,$$
$$\Delta_3 = \frac{1}{\sqrt{2}}\big(\psi^7_{+1/2}\uparrow - \psi^7_{-1/2}\downarrow\big),$$
$$\Delta_4 = \frac{1}{\sqrt{2}}\big(\psi^7_{+1/2}\uparrow + \psi^7_{-1/2}\downarrow\big),$$
$$\Delta_5 = \frac{1}{2}\big(\sqrt{3}\phi^8_{-1/2}\uparrow - \phi^8_{-3/2}\downarrow\big),$$
$$\frac{1}{2}\big(-\phi^8_{+3/2}\uparrow + \sqrt{3}\phi^8_{+1/2}\downarrow\big),$$
$$\Delta_3 = \frac{1}{\sqrt{2}}\big(\phi^8_{-3/2}\uparrow + \phi^8_{+3/2}\downarrow\big),$$
$$\Delta_1, \Delta_2 = \phi^8_{+1/2}\uparrow, \phi^8_{-1/2}\downarrow,$$
$$\Delta_5 = \frac{1}{2}\big(\phi^8_{-1/2}\uparrow + \sqrt{3}\phi^8_{-3/2}\downarrow\big),$$
$$\frac{1}{2}\big(\sqrt{3}\phi^8_{+3/2}\uparrow + \phi^8_{+1/2}\downarrow\big),$$

$$\Delta_4 = \frac{1}{\sqrt{2}}\left(\phi^8_{-3/2}\uparrow - \phi^8_{+3/2}\downarrow\right),$$

in the order of high to low energies, where some are degenerate in energy. The coupling coefficients for phonon-assisted recombination of these states are listed in Table II.

With inclusion of a finite δ_m, the coupling coefficients for the middle- and lowest-energy Δ_5 states deviate from the values in Table II. When a mass anisotropy splitting with the same amplitude as the exchange interactions ($\delta_m = E_{\rm ex}$) is assumed, we estimated that the lowest Δ_5 states acquire 10.9% of the oscillator strength of the middle Δ_5 states. The determination of the coefficients in the Hamiltonian will be discussed in our forthcoming publication.

[1] L. Childress and R. Hanson, MRS Bull. **38**, 134 (2013).
[2] C. J. Rauch, Phys. Rev. Lett. **7**, 83 (1961).
[3] P. J. Dean, E. C. Lightowlers, and D. R. Wight, Phys. Rev. **140**, A352 (1965).
[4] R. Sauer, H. Sternschulte, S. Wahl, K. Thonke, and T. R. Anthony, Phys. Rev. Lett. **84**, 4172 (2000).
[5] R. Sauer and K. Thonke, Phys. Rev. Lett. **86**, 3924 (2001).
[6] M. Cardona, T. Ruf, and J. Serrano, Phys. Rev. Lett. **86**, 3923 (2001).
[7] Y. Onodera and Y. Toyozawa, J. Phys. Soc. Jpn. **22**, 833 (1967).
[8] J. Serrano, A. Wysmolek, T. Ruf, and M. Cardona, Physica B **273**, 640 (1999).
[9] J. Serrano, M. Cardona, and T. Ruf, Solid State Commun. **113**, 411 (2000).
[10] N. Naka, K. Fukai, Y. Handa, and I. Akimoto, Phys. Rev. B **88**, 035205 (2013).
[11] N. O. Lipari and M. Altarelli, Phys. Rev. B **15**, 4883 (1977).
[12] S. J. Sharp, A. T. Collins, G. Davies, and G. S. Joyce, J. Phys.: Condens. Matter **9**, L451 (1997).
[13] N. Naka, T. Kitamura, J. Omachi, and M. Kuwata-Gonokami, Phys. Status Solidi B **245**, 2676 (2008).
[14] Y. Hazama, N. Naka, M. Kuwata-Gonokami, and K. Tanaka, Europhys. Lett. **104**, 47012 (2013).
[15] J. C. Merle, M. Capizzi, P. Fiorini, and A. Frova, Phys. Rev. B **17**, 4821 (1978).
[16] R. Pässler, Phys. Status Solidi B **216**, 975 (1999).
[17] G. F. Koster, J. O. Dimmock, R. G. Wheeler, and H. Statz, *Properties of the Thirty-Two Point Groups* (MIT Press, Cambridge, MA, 1963).
[18] D. L. Smith and T. C. McGill, Phys. Rev. B **14**, 2448 (1976).
[19] M. Willatzen, M. Cardona, and N. E. Christensen, Phys. Rev. B **50**, 18054 (1994).
[20] N. O. Lipari and A. Baldereschi, Phys. Rev. B **3**, 2497 (1971).
[21] J. Omachi, T. Suzuki, K. Kato, N. Naka, K. Yoshioka, and M. Kuwata-Gonokami, Phys. Rev. Lett. **111**, 026402 (2013).
[22] J. L. Warren, J. L. Yarnell, G. Dolling, and R. A. Cowley, Phys. Rev. **158**, 805 (1967).
[23] C. D. Clark, P. J. Dean, and P. V. Harris, Proc. R. Soc. A **277**, 312 (1964).
[24] Y. Toyozawa, *Optical Processes in Solids* (Cambridge University Press, Cambridge, UK, 2003).